LETTER

doi:10.1038/nature11882

Sensitivity of tropical carbon to climate change constrained by carbon dioxide variability

Peter M. Cox[1], David Pearson[2], Ben B. Booth[2], Pierre Friedlingstein[1], Chris Huntingford[3], Chris D. Jones[2] & Catherine M. Luke[1]

The release of carbon from tropical forests may exacerbate future climate change[1], but the magnitude of the effect in climate models remains uncertain[2]. Coupled climate–carbon-cycle models generally agree that carbon storage on land will increase as a result of the simultaneous enhancement of plant photosynthesis and water use efficiency under higher atmospheric CO_2 concentrations, but will decrease owing to higher soil and plant respiration rates associated with warming temperatures[3]. At present, the balance between these effects varies markedly among coupled climate–carbon-cycle models, leading to a range of 330 gigatonnes in the projected change in the amount of carbon stored on tropical land by 2100. Explanations for this large uncertainty include differences in the predicted change in rainfall in Amazonia[4,5] and variations in the responses of alternative vegetation models to warming[6]. Here we identify an emergent linear relationship, across an ensemble of models[7], between the sensitivity of tropical land carbon storage to warming and the sensitivity of the annual growth rate of atmospheric CO_2 to tropical temperature anomalies[8]. Combined with contemporary observations of atmospheric CO_2 concentration and tropical temperature, this relationship provides a tight constraint on the sensitivity of tropical land carbon to climate change. We estimate that over tropical land from latitude 30° north to 30° south, warming alone will release 53 ± 17 gigatonnes of carbon per kelvin. Compared with the unconstrained ensemble of climate–carbon-cycle projections, this indicates a much lower risk of Amazon forest dieback under CO_2-induced climate change if CO_2 fertilization effects are as large as suggested by current models[9]. Our study, however, also implies greater certainty that carbon will be lost from tropical land if warming arises from reductions in aerosols[10] or increases in other greenhouse gases[11].

We use results from the Coupled Climate Carbon Cycle Model Intercomparison Project[3] (C^{4}MIP) focusing on changes in tropical land carbon storage in the latitudinal band from 30° N to 30° S. Although C^{4}MIP included general circulation models (GCMs) and Earth-system models of intermediate complexity, we limit our analysis to the GCMs because our emergent constraint requires models that generate interannual variability. The C^{4}MIP experimental design[3] forced models using the SRES A2 scenario[12] of anthropogenic CO_2 emissions (including those due to land-use change). For each model, an 'uncoupled' simulation was carried out in which the land and ocean carbon cycles were made insensitive to the climate change caused by the increase in atmospheric CO_2. Comparison between the coupled and uncoupled simulations allows the direct effects of CO_2 on land and ocean carbon sinks to be separated from the effects of climate change[3,13]. We test the emergent constraint derived from the C^{4}MIP GCMs against results from the recent HadCM3 land carbon-cycle ensemble[14].

Our emergent constraint could also be tested against the recent CMIP5 climate–carbon-cycle models, which will appear in the Fifth Assessment Report of the Intergovernmental Panel on Climate Change. However, models in that report typically use prescribed concentrations of atmospheric CO_2 (ref. 15). This makes direct comparison with the observed interannual variability in the atmospheric CO_2 concentration difficult. Therefore, the emergent constraint we present here is conditional on the relatively simplistic representations of the carbon cycle in the C^{4}MIP models.

Table 1 summarizes results from six C^{4}MIP GCMs (A to F) for 1960 to 2099. For all models, the impact of climate change on the carbon cycle results in a larger increase in atmospheric CO_2 in the coupled simulation relative to the uncoupled simulation. This amplification varies by an order of magnitude across the model ensemble (from an extra 18 parts per million by volume (p.p.m.v.) in model D to an extra 212 p.p.m.v. in model A). A large part of this uncertainty arises from differing responses of tropical land carbon to projected climate changes in each model. All models produce a significant increase in tropical land carbon storage in the uncoupled simulations as a result of the direct effects of CO_2 on photosynthesis and water-use efficiency (from +263 gigatonnes of carbon (GtC) in model F to +413 GtC in model C). The neglect of carbon–nitrogen interactions in this first generation of climate–carbon models is arguably a major limitation in the mid and high latitudes[16], but is much less problematic in tropical forests, which are not typically nitrogen-limited[17]. Forest inventories are also consistent with a significant CO_2 fertilization in the tropics[18,19]. Despite the reasonable agreement among models on the effect of CO_2 fertilization, the fully coupled simulations produce very different changes in tropical land carbon storage from 1960 to 2099 (from −11 GtC for model A to +319 GtC for model D).

Figure 1a represents the evolution of tropical land carbon storage in the C^{4}MIP models, with the upper and lower estimates shown for both the coupled and uncoupled simulations. The lower estimate in the coupled simulation comes from the HadCM3LC model, which projects Amazon forest dieback under CO_2-induced climate change[1,9,10]. In this model, tropical land carbon storage increases owing to direct CO_2 effects until around 2050, but then declines abruptly owing to warming and drying in Amazonia[9]. This projection, along with recent extreme droughts in Amazonia[20–22], suggests that tropical forest dieback is a potential high-impact tipping element that would constitute an abrupt change in Earth's climate system[23].

To separate direct effects of CO_2 from those of climate change, we follow previous analyses[3,13] in writing the change in tropical land carbon storage, ΔC_{LT}, in terms of the change in atmospheric CO_2, ΔC_a, and the change in tropical mean temperature, ΔT_T:

$$\Delta C_{LT} = \beta_{LT}\Delta C_a + \gamma_{LT}\Delta T_T$$

Here β_{LT} (GtC per p.p.m.v.) and γ_{LT} (GtC K^{-1}) are the sensitivities of tropical land carbon storage to direct CO_2 effects and to climate change, respectively. The uncoupled simulations are used to estimate β_{LT} for each model, and then these values are used to isolate γ_{LT} from the coupled simulations[3,13] by subtracting the direct CO_2 effect. Figure 1b is a scatter plot of β_{LT} and γ_{LT} for each C^{4}MIP model and the three HadCM3 ensemble members. Whereas the β_{LT} values span a factor of two, from about 0.5 to 1 GtC per p.p.m.v., the γ_{LT} values range

[1]College of Engineering, Mathematics and Physical Science, University of Exeter, Exeter EX4 4QF, UK. [2]Hadley Centre, Met Office, Exeter EX1 3PB, UK. [3]Centre for Ecology and Hydrology, Wallingford OX10 8BB, UK.

Table 1 | Summary data for climate-carbon cycle projections

Model		Change in global atmospheric CO_2 (p.p.m.v.)		Change in tropical land carbon (GtC)		Change in tropical temperature (K)
		Coupled	Uncoupled	Coupled	Uncoupled	
A	HadCM3LC	689	477	−11	354	3.93
B	IPSL	453	381	177	365	2.70
C	MPI	524	443	242	413	4.36
D	CCSM1	483	465	319	364	1.53
E	FRCGC	589	465	118	271	3.61
F	LOOP	489	460	185	263	3.30
G	HadCM3C-st	599	331	−148	317	4.41
H	HadCM3C-a	445	333	−6	168	3.76
I	HadCM3C-h	589	246	−165	251	4.08

Changes in atmospheric CO_2, tropical land carbon and tropical near-surface air temperature (30° N–30° S), as simulated by the nine climate–carbon GCMs analysed in this study. Models A to F are from the C^{4}MIP study[3], which prescribed the SRES A2 CO_2 emissions scenario. For these models, the changes are calculated over the period 1960–2099. Models G to I are from a land carbon-cycle parameter ensemble carried out with the HadCM3 model under the SRES A1B scenario[14], and were run only to 2080, so differences here are for 1960 to 2080. In all cases, model runs were carried out both including and excluding climate effects on the carbon cycle ('coupled' and 'uncoupled', respectively), so that the impacts of climate–carbon-cycle feedbacks could be diagnosed.

over a factor of more than four, from $-29\,\mathrm{GtC\,K^{-1}}$ (model F) to $-133\,\mathrm{GtC\,K^{-1}}$ (model A), with a C^{4}MIP mean of $-69\,\mathrm{GtC\,K^{-1}}$ and standard deviation of $39\,\mathrm{GtC\,K^{-1}}$. This range is even larger if the HadCM3 ensemble members are included. We therefore focus on reducing the larger uncertainty, namely that in γ_{LT}.

Our inspiration for deriving a multi-model emergent constraint comes from a recent study that showed a strong relationship between the contemporary temperature sensitivity of seasonal snow cover and the magnitude of the snow–albedo feedback, across more than 20 GCMs[7]. Because the seasonal cycle of snow cover can be estimated from observations, this model-derived relationship converts the contemporary observations to a constraint on the size of the snow–albedo feedback in the real climate system, for which there is no direct reliable measurement. Emergent constraints of this type make use of the often bewildering spread among Earth-system model projections to reduce uncertainties in the sensitivities of the real Earth system to anthropogenic forcing. They are distinct and complementary to bottom-up constraints arising from process-based studies.

It made sense a priori to look for an emergent constraint linking the sensitivity of tropical land carbon to interannual variability (IAV) in the growth rate of atmospheric CO_2. Tropical land carbon changes in response to climate through changes in the net land–atmosphere CO_2 flux into and out of this carbon store. Critically, the sensitivity of this net tropical CO_2 flux is revealed by the IAV in the CO_2 growth rate, because this is known to be dominated by the response of the tropical land carbon cycle to climatic anomalies (Supplementary Fig. 1a) such as the El Niño/Southern Oscillation[8,24,25]. Hence, some relationship between the IAV in CO_2 and the longer-term sensitivity of tropical land carbon storage to climate change (γ_{LT}) is to be expected, as long as processes that are not evident in the short-term variation of the CO_2 fluxes (for example forest dynamics or changes in long-lived soil carbon pools) do not dominate the long-term response. This is our working hypothesis to be tested against the C^{4}MIP models, which include a range of representations of slow vegetation and soil processes[3].

Figure 2a compares the observed IAV in the growth rate of global atmospheric CO_2 (refs 26, 27) with the IAV in the annual mean tropical temperature[28]. In both cases, we have chosen observational variables (global mean atmospheric CO_2 and mean land-plus-ocean temperature between 30° N and 30° S) for consistency with the variables available from the C^{4}MIP models. Aside from the years immediately after the volcanic eruptions[24] of Mount Agung, El Chichon and Mount Pinatubo, the IAV in the growth rate of atmospheric CO_2 is linearly correlated with the IAV in the tropical temperature ($r = 0.65$ (correlation coefficient), $P < 0.0001$; Fig. 2b), with a best-fit 'IAV sensitivity' of $5.1 \pm 0.9\,\mathrm{GtC\,yr^{-1}\,K^{-1}}$. Excluding these volcano-affected years has an impact on the best-fit sensitivity of less than 5%, but avoids the complication of diffuse-light fertilization of plant growth[29], which is not included in any of the C^{4}MIP models. We also find a similar sensitivity regardless of which tropical temperature reconstruction we use. There is a greater sensitivity to the choice of the global atmospheric CO_2 data set, but this does not affect our overall conclusions (Supplementary Table 1).

A similar calculation is made for each of the coupled climate–carbon-cycle models, to derive the sensitivity of the CO_2 growth rate to tropical temperature for the period 1960–2010. Compared with the observational data, models tend to overestimate the IAV in the tropical temperature by a factor of up to two, and to overestimate the IAV in the CO_2 growth rate by a factor of up to three. The correlation between these variables is underestimated in some models (F, B and D) and overestimated in others (A, E and C). Hence, IAV sensitivity varies across the C^{4}MIP model ensemble, from $2.9 \pm 1.4\,\mathrm{GtC\,yr^{-1}\,K^{-1}}$ (model F) to $9.7 \pm 0.7\,\mathrm{GtC\,yr^{-1}\,K^{-1}}$ (model A), with most of this range resulting from differences in the sensitivity of heterotrophic respiration to climate (Supplementary Fig. 1b). The three HadCM3

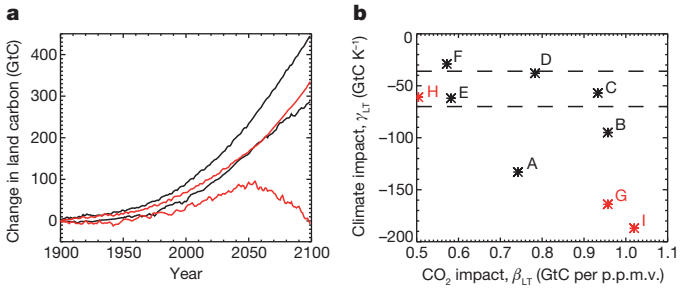

Figure 1 | Projected changes in land carbon storage in the tropics from coupled climate–carbon-cycle models. **a**, Upper and lower estimates from the C^{4}MIP models[3] (A–F in Table 1) for uncoupled (black lines) and coupled simulations (red lines). **b**, Impact of changes in tropical temperature versus impact of changes in atmospheric CO_2 on tropical land carbon, for the C^{4}MIP models (black letters) and three variants of the HadCM3C model[14] (red letters). The horizontal lines represent the new constraint presented in this study.

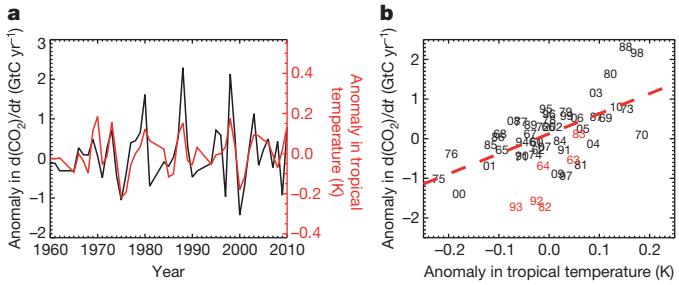

Figure 2 | Observed relationship between variations in the growth rate of atmospheric CO_2 and tropical temperature. **a**, Annual anomalies in CO_2 growth rate (black) and tropical temperature (red) versus year. **b**, Sensitivity of CO_2 growth rate to tropical temperature, with numbers representing the individual years in **a** and the dashed line showing the best-fit straight line, which has a gradient of $5.1 \pm 0.9\,\mathrm{GtC\,yr^{-1}\,K^{-1}}$. The years in red were not included in this fit because they directly followed major volcanic perturbations to the climate.

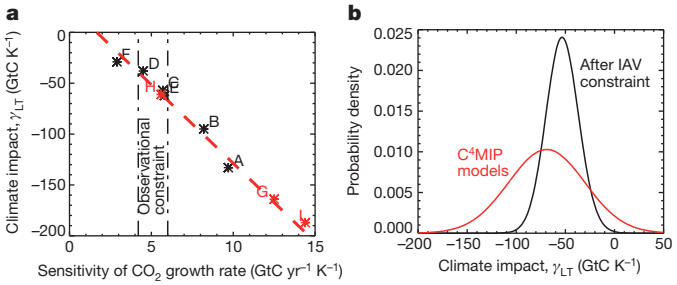

Figure 3 | Emergent constraint on the sensitivity of tropical land carbon to climate change. **a**, Climate sensitivity of tropical land carbon (γ_{LT}) versus the sensitivity of the CO_2 growth rate to tropical temperature, for each of the models shown in Table 1. The dashed line shows the best-fit straight line across the C^{4}MIP models (black). The red symbols represent a test of this relationship against the three HadCM3C ensemble members. The dot–dash lines indicate the constraint on the observed IAV in the CO_2 growth rate derived from Fig. 2b. **b**, PDF for the climate sensitivity of γ_{LT}. The black line was derived by applying the IAV constraint to the across-model relationship shown in **a**. The red line shows the 'prior' PDF that arises from assuming that all of the C^{4}MIP models are equally likely to be correct and that they come from a Gaussian distribution.

ensemble members, which were produced by perturbing only parameters in the land carbon-cycle component of the model[13], span an even larger range (5.6–14.4 GtC yr^{-1} K^{-1}), suggesting that uncertainties in the modelling of the tropical land carbon cycle are critical.

Most importantly, these differing IAV sensitivities are strongly correlated ($r = 0.98$, $P = 0.0005$) with variations in γ_{LT} across C^{4}MIP models (black labels in Fig. 3a). The dashed red line in Fig. 3a shows the best-fit straight line relating these variables for the six C^{4}MIP GCMs (although in principle a well-defined nonlinear function would also yield an emergent constraint). The red labels in Fig. 3a show how well this relationship would have predicted the variation in γ_{LT} for the three HadCM3 ensemble members given the IAV sensitivity of each. We note that two of the HadCM3 variants have γ_{LT} values beyond the range of the C^{4}MIP models, but that the extrapolated straight line is nevertheless able to fit these outliers. The dotted vertical black lines in Fig. 3a show the IAV sensitivity (± 1 s.d.), as previously estimated from the contemporary observations, from which we derive tighter bounds on γ_{LT}.

With the model-derived relationship between γ_{LT} and the IAV sensitivity, we can use the observational constraint to estimate a probability density function (PDF) for γ_{LT} (Methods). Figure 3b compares this with the PDF arising from assuming that all C^{4}MIP models are equally likely to be true and come from an underlying Gaussian distribution (red line). The emergent constraint from the IAV sensitivity of the CO_2 growth rate sharpens the PDF of γ_{LT} and moves its peak to a less negative value (-53 ± 17 as opposed to -69 ± 39 GtC K^{-1}). The application of the IAV constraint reduces the estimated probability of γ_{LT} values more negative than -100 GtC K^{-1}, typically associated with models that project CO_2-induced tropical forest dieback, by almost two orders of magnitude from 21% to 0.24%.

The IAV constraint also gives strong confirmation that tropical land carbon is vulnerable to warming caused by non-CO_2 forcing factors[11]. Remaining uncertainties in tropical land climate–carbon-cycle feedbacks are therefore the magnitude of long-term CO_2 fertilization effects in the tropics, and the extent to which future climate change will be caused by non-CO_2 factors.

METHODS SUMMARY

We used results from six of the eleven models used in C^{4}MIP[3]. The five excluded models consisted of four Earth-system models of intermediate complexity, which do not typically generate internal variability as required to define the interannual sensitivity of the CO_2 growth rate to tropical temperature anomalies, and one GCM (LLNL), which reported zonal mean land temperatures rather than zonal mean (land and ocean) temperatures. Outputs from the remaining six models were reported as annual means for each 30° latitudinal band (available at https://c4mip.lsce.ipsl.fr/diagnostics_phase2.html). We combined the outputs from the 30° N–0° and 0°–30° S bands to define the projected changes for the 30° N–30° S 'tropical' band.

Models G, H and I in this study, which are used to test the emergent constraint derived from the C^{4}MIP models, come from a land carbon-cycle ensemble carried out with the HadCM3C model[14]. HadCM3C is similar to C^{4}MIP model A (HadCM3LC) but includes a higher-resolution ocean model ($1.25° \times 1.25°$ rather than $2.5° \times 3.75°$) and interactive atmospheric sulphur-cycle chemistry. Seventeen HadCM3C ensemble members were defined by perturbations to key land surface parameters including leaf nitrogen concentrations and the temperature sensitivities of photosynthesis and soil respiration[14]. All ensemble members were driven by the SRES A1B emissions scenarios, including changes in non-CO_2 forcing factors (most notably changes in anthropogenic sulphate aerosols[10]). Uncoupled simulations were carried out only for the standard parameter values (HadCM3-st), and the ensemble members leading to the lowest (HadCM3-a) and highest (HadCM3-h) global carbon-cycle feedbacks. We therefore focused on these three variants of HadCM3C in this study.

The analysis of the model outputs and observational data, and the statistical methods employed are outlined in Methods.

Full Methods and any associated references are available in the online version of the paper.

Received 31 May; accepted 28 December 2012.
Published online 6 February 2013.

1. Cox, P. M., Betts, R. A., Jones, C. D., Spall, S. A. & Totterdell, I. J. Acceleration of global warming due to carbon cycle feedbacks in a coupled climate model. *Nature* **408,** 184–187 (2000).
2. Malhi, Y. *et al.* Climate change, deforestation, and the fate of the Amazon. *Science* **319,** 169–172 (2008).
3. Friedlingstein, P. *et al.* Climate-carbon cycle feedback analysis: results from the C^{4}MIP model intercomparison. *J. Clim.* **19,** 3337–3353 (2006).
4. Jupp, T. E. *et al.* Development of probability density functions for future South American rainfall. *New Phytol.* **187,** 682–693 (2010).
5. Rammig, A. *et al.* Estimating the risk of Amazonian forest dieback. *New Phytol.* **187,** 694–706 (2010).
6. Galbraith, D. *et al.* Multiple mechanisms of Amazonian forest biomass losses in three dynamic global vegetation models under climate change. *New Phytol.* **187,** 647–665 (2010).
7. Hall, A. & Qu, X. Using the current seasonal cycle to constrain snow albedo feedback in future climate change. *Geophys. Res. Lett.* **33,** L03502 (2006).
8. Bacastow, R. Modulation of atmospheric carbon dioxide by the Southern Oscillation. *Nature* **261,** 116–118 (1976).
9. Cox, P. M. *et al.* Amazon dieback under climate-carbon cycle projections for the 21st century. *Theor. Appl. Climatol.* **78,** 137–156 (2004).
10. Cox, P. M. *et al.* Increasing risk of Amazonian drought due to decreasing aerosol pollution. *Nature* **453,** 212–215 (2008).
11. Huntingford, C. *et al.* Highly contrasting effects of different climate forcing agents on ecosystem services. *Phil. Trans. R. Soc. A* **369,** 2026–2037 (2011).
12. Nakicenovic, N. *et al. Emissions Scenarios: Summary for Policymakers*. Spec. Report (Intergovernmental Panel on Climate Change, 2000).
13. Friedlingstein, P., Dufresne, J.-L., Cox, P. M. & Rayner, P. How positive is the feedback between climate change and the carbon cycle? *Tellus* **55B,** 692–700 (2003).
14. Booth, B. B. B. *et al.* High sensitivity of future global warming to land carbon cycle processes. *Environ. Res. Lett.* **7,** 024002 (2012).
15. Moss, R. H. *et al.* The next generation of scenarios for climate change research and assessment. *Nature* **463,** 747–756 (2010).
16. Hungate, B. A. *et al.* Nitrogen and climate change. *Science* **302,** 1512–1513 (2003).
17. Zaehle, S., Friedlingstein, P. & Friend, A. D. Terrestrial nitrogen feedbacks may accelerate future climate change. *Geophys. Res. Lett.* **37,** L01401 (2010).
18. Baker, T. R. *et al.* Increasing biomass in Amazonian forest plots. *Phil. Trans. R. Soc. Lond. B* **359,** 353–365 (2004).
19. Lewis, S. L. *et al.* Increasing carbon storage in intact African tropical forests. *Nature* **457,** 1003–1006 (2009).
20. Marengo, J. A. *et al.* The drought of Amazonia in 2005. *J. Clim.* **21,** 495–516 (2008).
21. Marengo, J. A. *et al.* The drought of 2010 in the context of historical droughts in the Amazon region. *Geophys. Res. Lett.* **38,** L12703 (2011).
22. Phillips, O. *et al.* Drought sensitivity of the Amazon rainforest. *Science* **323,** 1344–1347 (2009).
23. Lenton, T. M. *et al.* Tipping elements in the Earth's climate system. *Proc. Natl Acad. Sci. USA* **105,** 1786–1793 (2008).
24. Jones, C. D. & Cox, P. M. On the significance of atmospheric CO_2 growth rate anomalies in 2002–2003. *Geophys. Res. Lett.* **32,** L14816 (2005).
25. Denman, K. L. *et al.* in *Climate Change 2007: The Physical Science Basis* (eds Solomon, S. *et al.*) 499–587 (Cambridge Univ. Press, 2007).
26. Masarie, K. A. & Tans, P. P. Extension and integration of atmospheric carbon dioxide data into a globally consistent measurement record. *J. Geophys. Res.* **100,** 11593–11610 (1995).
27. Meinshausen, M. *et al.* The RCP greenhouse gas concentrations and their extensions from 1765 to 2500. *Clim. Change* **109,** 213–241 (2011).

28. Smith, T. M. *et al.* Improvements to NOAA's historical merged land-ocean surface temperature analysis (1880–2006). *J. Clim.* **21,** 2283–2296 (2008).
29. Mercado, L. M. *et al.* Impact of changes in diffuse radiation on the global land carbon sink. *Nature* **458,** 1014–1017 (2009).

Supplementary Information is available in the online version of the paper.

Acknowledgements We acknowledge funding from the NERC NCEO programme (P.M.C. and C.M.L.); the EU Greencycles II project (P.M.C. and P.F.); the EU FP7 'CARBONES' project (D.P. and C.D.J.); the Joint DECC/Defra Met Office Hadley Centre Climate Programme (GA01101) (D.P., B.B.B. and C.D.J.); the CEH Science Budget (C.H.) and the Newton Institute programme on 'Mathematical and Statistical Approaches to Climate Modelling and Prediction', during which this research was first formulated (P.M.C., B.B.B. and C.H.). We also acknowledge the modelling groups that provided results to C^4MIP.

Author Contributions P.M.C. led the study and drafted the manuscript. D.P. assisted with the statistical analysis, especially the estimation of the observationally constrained PDF in Fig. 3b. P.F. provided data and guidance on the C^4MIP model ensemble, and B.B.B. did likewise for the HadCM3 carbon-cycle ensemble. C.H. processed observational climate data sets to produce time series of tropical mean temperature anomalies. P.M.C., C.D.J., P.F. and C.H. have had discussions over many years concerning the relationship between the interannual variability and the long-term sensitivity of the land carbon cycle to climate change. C.M.L. provided invaluable insights into the interpretation of the regression line in Fig. 3a. All co-authors commented on and provided edits to the original manuscript.

Author Information Reprints and permissions information is available at www.nature.com/reprints. The authors declare no competing financial interests. Readers are welcome to comment on the online version of the paper. Correspondence and requests for materials should be addressed to P.M.C. (p.m.cox@exeter.ac.uk).

METHODS

Choice of models and variables. To make use of the observed interannual variation in atmospheric CO_2 as a constraint, we need climate–carbon-cycle simulations that model CO_2 as a 'free', fully prognostic variable. We therefore make use of the C^{4}MIP simulations[3], which used prescribed SRES A2 CO_2 emissions but calculated the global mean atmospheric CO_2 concentration interactively. We have augmented the C^{4}MIP results with free CO_2 runs from a carbon-cycle parameter ensemble carried out with HadCM3 (ref. 14). These HadCM3 runs allow the emergent constraint derived from the C^{4}MIP models to be tested over a wide range of possible future carbon losses from tropical land.

To derive an emergent constraint, it is of paramount importance that equivalent variables are compared from the models and observations. Therefore, because the C^{4}MIP models reported global mean atmospheric CO_2, and mean land-plus-ocean near-surface temperatures, we compute the same diagnostics from the observational data sets (see below).

Diagnosis of γ_{LT}. The sensitivity of tropical land carbon storage to temperature, γ_{LT}, is calculated as in previous studies[3,13]. First, the sensitivity of tropical land carbon storage to direct CO_2 effects, as given by the parameter β_{LT}, is diagnosed from the uncoupled simulation for each model, $\beta_{LT} = \Delta C^u_{LT}/\Delta C^u_a$, where $\Delta C^u_{LT} = C^u_{LT}(t_1) - C^u_{LT}(t_0)$ is the change in tropical land carbon storage (in GtC) and $\Delta C^u_a = C^u_a(t_1) - C^u_a(t_0)$ is the change in global atmospheric CO_2 concentration (in p.p.m.v.), in both cases between time t_0 and time t_1 for the uncoupled simulation.

This value of β_{LT} is then used to isolate γ_{LT} from the coupled simulation of each model, using the equation

$$\gamma_{LT} = \frac{\Delta C^c_{LT} - \beta_{LT}\Delta C^c_a}{\Delta T^c_T}$$

where $\Delta C^c_{LT} = C^c_{LT}(t_1) - C^c_{LT}(t_0)$ is the change in tropical land carbon storage (in GtC), $\Delta C^c_a = C^c_a(t_1) - C^c_a(t_0)$ is the change in global atmospheric CO_2 concentration (in p.p.m.v.) and $\Delta T^c_T = T^c_T(t_1) - T^c_T(t_0)$ is the change in mean tropical (30° N–30° S) temperature (in K), in all cases between time t_0 and time t_1 for the coupled simulation.

We define the changes relative to 1960 in all cases (that is, $t_0 = 1960$), and use the longest possible common simulation periods over which to diagnose β_{LT} and γ_{LT} for the C^{4}MIP models ($t_1 = 2099$) and the HadCM3C ensemble members ($t_1 = 2080$), respectively.

Sensitivity of CO_2 growth-rate anomaly to tropical temperature anomaly. The sensitivity of the atmospheric CO_2 growth rate to tropical temperature is calculated over the period 1960–2010 inclusive, for the observations and all models. However, for the observational data, and the HadCM3C simulations, which included volcanoes, we exclude the years 1963, 1964, 1982, 1983, 1991 and 1992, which were heavily influenced by the volcanic eruptions[24] of Mount Agung (in 1963), El Chichon (in 1982) and Mount Pinatubo (in 1991). There are two reasons for removing volcanoes. First, not all the models in our ensembles include the climatic effects of volcanic eruptions. Second, volcanoes are believed to affect the land carbon sink through the effects of diffuse radiation fertilization[29], but these effects are not included in the generation of models considered here. We therefore removed 'volcano years' from the observations to maximize consistency between models and observations.

For comparability with the outputs available from the C^{4}MIP models, we also use the global CO_2 concentration and the mean tropical (30° N–30° S) temperature, including both land and ocean points.

As in previous studies[24], the annual CO_2 growth rate for the nth year, $dC_a/dt(t_n)$, is defined as the difference between the annual mean CO_2 concentrations for the nth and $(n-1)$th years: $dC_a/dt(t_n) = C_a(t_n) - C_a(t_{n-1})$. The CO_2 growth rate is therefore centred in time at the beginning of year n. To align the tropical temperature anomalies, we take the associated tropical mean temperature, $\bar{T}_T(t_n)$, to be the mean of the annual mean tropical temperatures for years n and $n-1$:

$$\bar{T}_T(t_n) = \frac{T_T(t_n) + T_T(t_{n-1})}{2}$$

For all model and observational time series, the annual CO_2 growth rate, dC_a/dt, and the associated mean tropical temperature, $\bar{T}_T$, were detrended using an 11-yr running mean, with the residuals defining the annual anomalies (Supplementary Fig. 2). In each case, a least-squares linear regression was found between these anomalies in the CO_2 growth rate and the anomalies in the tropical temperature, with the gradient of the best fit defining the IAV sensitivity (see below).

The IAV sensitivity was calculated for a range of data sets of tropical temperature and atmospheric CO_2 (see below), to explore the uncertainty in the estimate of the IAV sensitivity arising from uncertainties in the observational data. These different estimates are listed in Supplementary Table 1.

To isolate the separate contributions of the tropical net primary productivity and soil respiration, similar regressions against tropical temperature anomalies were carried out separately for each of these fluxes as diagnosed from the C^{4}MIP models (Supplementary Fig. 1). This showed that the IAV sensitivity across the model ensemble is correlated with the response of tropical soil respiration (Supplementary Fig. 1b), rather than net primary productivity (Supplementary Fig. 1c). By contrast, the wide range of longer-term projections of changes in land carbon storage is known to be in part due to the different responses of net primary productivity to climate change[3].

Observational data. Observed annual global CO_2 concentration[26] for 1980 to 2010 was downloaded from the NOAA website (http://www.esrl.noaa.gov/gmd/ccgg/trends/global.html#global_data). Because this data set covers only the period from 1980, global CO_2 concentrations for 1960–1979 were taken from the historical data sets derived for use with the RCP scenarios[27] (http://www.pik-potsdam.de/~mmalte/rcps/index.htm#).

Tropical (30° N–30° S) annual mean temperatures were calculated from NCDC data[28] (http://www.ncdc.noaa.gov/ghcnm/maps.php), from the CRU/Met Office HadCRU3 data set (http://www.metoffice.gov.uk/hadobs/hadcrut3/) and from the GISS data set (http://data.giss.nasa.gov/gistemp/).

Least-squares linear regression. Least-squares linear regressions were calculated using well-established formulae (see, for example, http://mathworld.wolfram.com/LeastSquaresFitting.html). The linear regression, f_n, between a time series given by y_n and a time series given by x_n is defined by a gradient, b, and intercept, a: $f_n = a + bx_n$. Minimizing the least squares error for y_n involves minimizing

$$s^2 = \frac{1}{N-2}\sum_{n=1}^{N}\{y_n - f_n\}^2$$

where N is the number of data points in each time series. In this case, the best-fit gradient is given by $\bar{b} = \sigma^2_{xy}/\sigma^2_x$. Here $\sigma^2_x = \sum_{n=1}^{N}\{x_n - \bar{x}\}^2/N$ is the variance of x_n and $\sigma^2_{xy} = \sum_{n=1}^{N}\{x_n - \bar{x}\}\{y_n - \bar{y}\}/N$ is the covariance of the x_n and y_n time series, which have means of $\bar{x}$ and $\bar{y}$, respectively. The standard error of b is given by $\sigma_b = s/\sigma_x\sqrt{N}$, which defines a Gaussian probability density for b:

$$P(b) = \frac{1}{\sqrt{2\pi\sigma^2_b}}\exp\left\{-\frac{(b-\bar{b})^2}{2\sigma_b}\right\}$$

The 'prediction error' of the regression is the following function of x:

$$\sigma_f(x) = s\sqrt{1 + \frac{1}{N} + \frac{(x-\bar{x})^2}{N\sigma^2_x}}$$

This expression defines contours of equal probability density around the best-fit linear regression, which represent the probability density of y given x:

$$P\{y|x\} = \frac{1}{\sqrt{2\pi\sigma^2_f}}\exp\left\{-\frac{(y-f(x))^2}{2\sigma_f}\right\}$$

where $\sigma_f = \sigma_f(x)$, as above.

Calculation of the PDF for γ_{LT}. The emergent constraint derived in this study is a linear regression across the C^{4}MIP GCMs between the temperature sensitivity of land carbon storage in the tropics, γ_{LT}, and the sensitivity of the annual growth rate in atmospheric CO_2 to the annual tropical temperature anomaly, which we label here as γ_{CO2}. In the context of the least-squares linear regression presented above, γ_{LT} is equivalent to y and γ_{CO2} is equivalent to x.

The linear regression therefore provides an equation for the probability of γ_{LT} given γ_{CO2} (that is, the equation for $P\{y \mid x\}$ above). Supplementary Fig. 3 shows the best-fit straight line (thick dashed red line) and the plus and minus σ_f prediction error contours (as thin dashed red lines) on the same scales as in Fig. 3a.

In addition, the linear regression between the observed annual anomalies in the atmospheric CO_2 growth rate[25,26] and the tropical mean temperature[27] provides an observation-based PDF for γ_{CO2} (via the equation for $P(b)$ above). The best-fit γ_{CO2} from these observations is shown by the thick dashed vertical line in Supplementary Fig. 3, and the uncertainty in this fit is shown by the thin dashed vertical lines representing plus and minus 1 s.e. about the best-fit value.

Given these two PDFs, $P\{\gamma_{LT} \mid \gamma_{CO2}\}$ and $P(\gamma_{CO2})$, the PDF for γ_{LT} is

$$P(\gamma_{LT}) = \int_{-\infty}^{\infty} P\{\gamma_{LT}|\gamma_{CO2}\}P(\gamma_{CO2})\,d\gamma_{CO2}$$

The integrand, $P\{\gamma_{LT}|\gamma_{CO2}\}P(\gamma_{CO2})$, is shown by the continuous black contours in Supplementary Fig. 3, and the integral is the basis for the black PDF for γ_{LT} shown in Fig. 3b.